Available online at www.sciencedirect.com

ScienceDirect

Mendeleev Commun., 2022, **32**, 571–575

Mendeleev Communications

A computational mapping of the R–NHC coupling pathway – the key process in the evolution of Pd/NHC catalytic systems

Alexander Yu. Kostyukovich, Evgeniy G. Gordeev and Valentine P. Ananikov*

N. D. Zelinsky Institute of Organic Chemistry, Russian Academy of Sciences, 119991 Moscow, Russian Federation. E-mail: val@ioc.ac.ru

DOI: 10.1016/j.mencom.2022.09.001

C–C coupling reactions are of great importance in metal-catalyzed synthetic transformations. Reductive elimination of two carbon centers is the key stage, which takes place in the metal coordination sphere. In the present study, we provide a detailed analysis of nonclassical R–NHC coupling in the model (NHC)Pd^{II}(Ph)(X)(Solv) complex, which is a representative intermediate of the Mizoroki–Heck and cross-coupling reactions. This C–C bond formation stage proceeds as Ph ligand movement and insertion into the Pd–NHC bond, rather than classical C–C coupling. Based on the analysis by the quantum theory of atoms in molecules (QTAIM) of the reaction path structures, the atomic rearrangements and alterations in the electronic system during the R–NHC coupling process were characterized in detail.

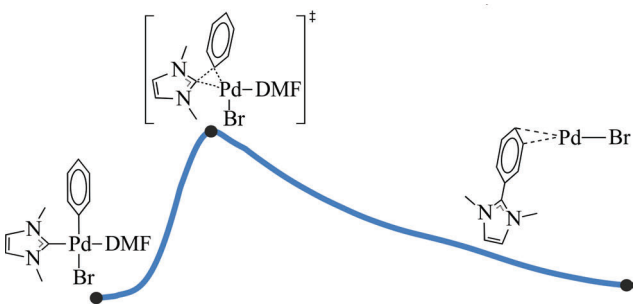

Keywords: R–NHC coupling, DFT calculations, reaction mechanism, palladium catalysis, catalyst evolution.

Since it was shown that N-heterocyclic carbenes (NHCs), isolated and characterized in 1991 by Arduengo *et al.*,[1] can act as auxiliary ligands in metal complex catalysts,[2] a vast number of M/NHC-based catalytic systems have been developed.[3] In particular, palladium complexes with NHC ligands have found wide application as universal catalysts operating in a large number of synthetic transformations.[4] The variety of NHCs and the great potential for their structural modification allow fine-tuning of the activity, selectivity, stability, and other important parameters of catalytic systems. Due to the pronounced electron donating properties of these ligands, the Pd–NHC bond is strong, and the complexes are often considered well-defined.[5] The coupling process involving NHC ligands was studied previously,[6] but the role in the catalytic process was not addressed.

Recently, we discovered that the R–NHC coupling process changes the mode of the catalytic system and results in the appearance of nanocatalysis.[7] Such unconventional coupling occurs in key intermediates of the cross-coupling and Mizoroki–

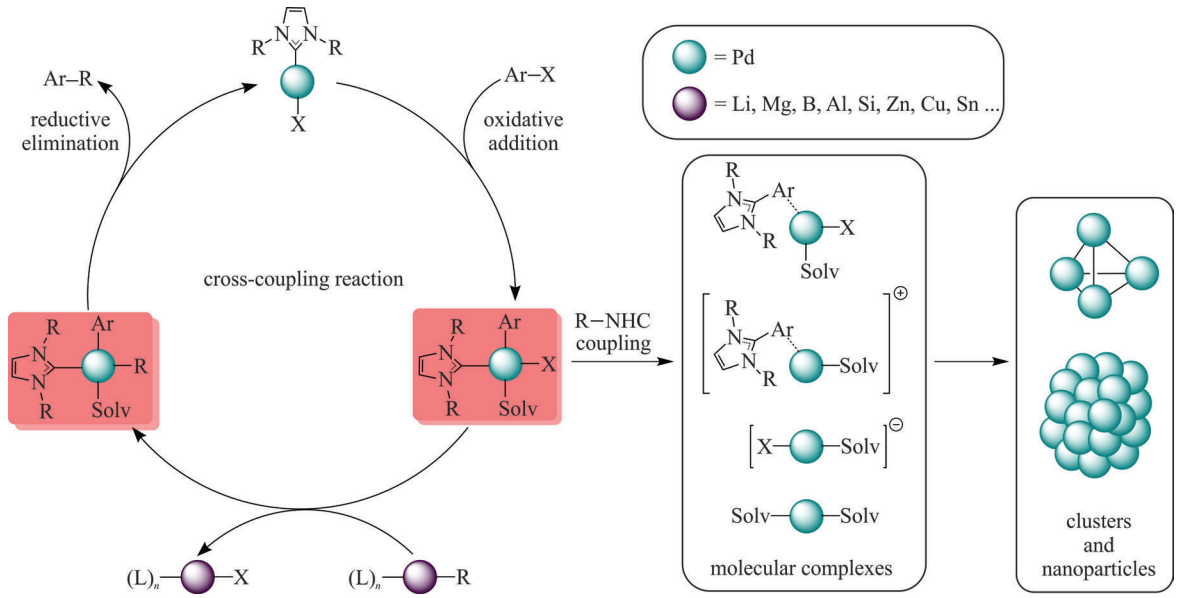

Scheme 1 Evolution of the Pd/NHC catalytic system in cross-coupling reactions.

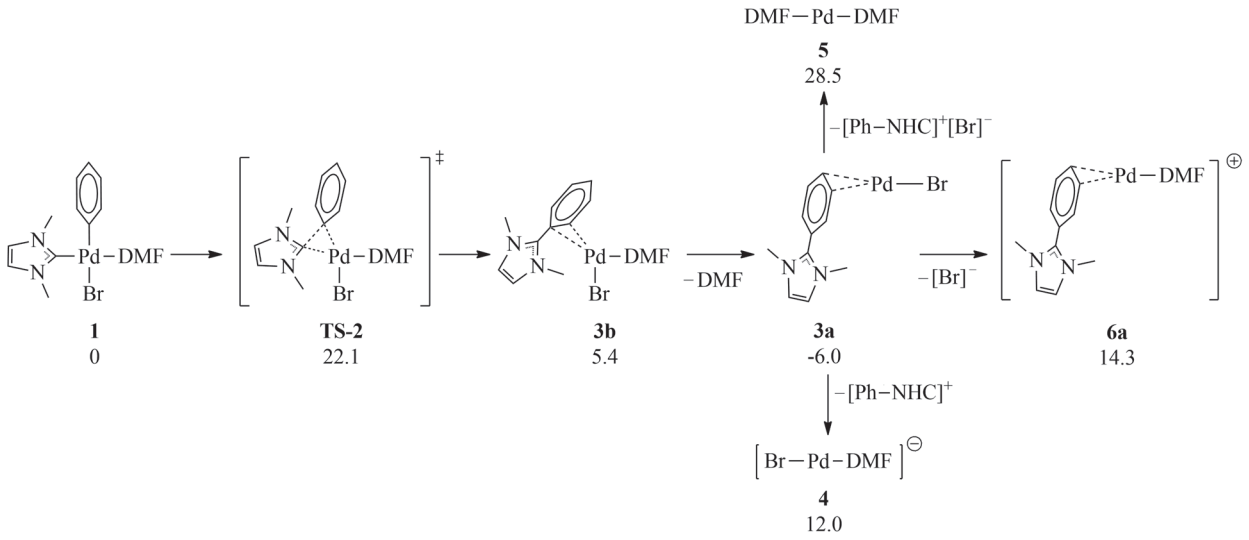

Scheme 2 Free energies Δ*G* (kcal mol^{-1}) of the R–NHC coupling and subsequent ligand exchange reactions. PBE1PBE-GD3BJ/Def2-TZVP SMD(DMF) level of theory.

Heck reactions and results in Pd–NHC bond cleavage (Scheme 1). R–NHC coupling is a key process in the evolution of catalytic systems that results in a wide variety of palladium-containing compounds in the reaction system.[8]

This article provides the results of a theoretical study of the Pd–NHC coupling reaction and subsequent release of catalytically active NHC-free Pd^0 species. The influence of the entropy factor and the solvent medium on this process was evaluated. A detailed analysis of the reaction coordinate has been made. Based on QTAIM, the key points for the formation and breaking of chemical bonds along the reaction path have been determined.

Quantum-chemical calculations of the R–NHC coupling reaction in the gas phase (GP) and in continuum solvent models were carried out (Table 1).† The Polarizable continuum model (PCM)[9] and the continuum solvation model based on the quantum mechanical charge density (SMD)[10] were used to take into account the solvent effect on the process under consideration. *N*,*N*-Dimethylformamide (DMF) was chosen as the solvent in both cases. Palladium complex **1** was taken as a model system (Scheme 2). The activation energy $\Delta G^{\ddagger}$ of process **1** → **TS-2** is low and varies in a narrow range from 22.1 (SMD) to 23.4 (GP) kcal mol^{-1}. Product **3b** has a square planar configuration, which is not typical for the Pd^0 complex. Indeed, the dissociation of the solvate ligand with the formation of a linear structure **3a** lowers the energy of the system. The stabilization of compound **3** is much more pronounced in a polar medium than in the gas phase. Thus, Δ*G* (**3b** → **3a**) in the framework of the SMD model is −11.4 kcal mol^{-1} (−9.6 for PCM), while in the gas phase, this parameter is −1.5 kcal mol^{-1}. The solvent also has a great influence on the thermodynamics of R–NHC coupling **1** → **3a**. This reaction is endergonic in the gas phase (Δ*G* = 9.7 kcal mol^{-1}), and in a polar medium, it becomes energetically favorable (Δ*G* = −3.3 and −6.0 kcal mol^{-1} for the PCM and SMD calculations, respectively). Such a large difference in the energy values can be explained by the significant charge separation in compound **3a**, which consists of the cationic [Ph–NHC]$^+$ and anionic [Pd–Br]$^-$ parts. Thus, the Mulliken charge of the Ph–NHC fragment in product **3a** is 0.68 a.u. (see below). This compound can be considered a salt. For this reason, solvation significantly stabilizes complex **3a** in a polar medium.

Table 1 Thermodynamic parameters (kcal mol^{-1}) of the R–NHC coupling obtained in various model systems. PBE1PBE-GD3BJ/Def2-TZVP level of theory.

	GP,[a] Δ*G*	PCM,[b] Δ*G*	SMD[b]		
			Δ*H*	Δ*G*	*T*Δ*S*
1	0	0	0	0	0
TS-2	23.4	22.3	21.2	22.1	−0.9
3b	11.2	6.3	5.0	5.4	−0.4
3a	9.7	−3.3	3.9	−6.0	9.9
4	108.7	15.3	23.5	12.0	11.5
5	43.1	26.6	37.0	28.5	8.5
6a	98.2	10.2	22.0	14.3	7.7

[a] Gas phase. [b] DMF was chosen as the solvent in continuum models.

Compound **3a** can further enter into ligand exchange reactions to form anionic **4**, neutral **5**, and cationic **6a** complexes. However, these reactions are unfavorable if a DMF molecule is considered a substituting ligand. According to SMD calculations, among the various pathways of ligand exchange, the formation of anionic compound **4** has the lowest energy (Δ*G* = 18.0 kcal mol^{-1}). The formation energy of cationic complex **6a** is slightly higher (Δ*G* = 20.3 kcal mol^{-1}). The least favorable is the formation of palladium with two solvate ligands **5** (Δ*G* = 34.5 kcal mol^{-1}). Another order of stability of the ligand exchange products was obtained in the framework of the PCM calculations: **6a** (13.5) > **4** (18.6) > **5** (29.9 kcal mol^{-1}). Calculations in the gas phase showed that the processes in complex **3b** are extremely unfavorable, especially if charged complexes are formed.

Table 1 shows the relative values of the thermodynamic parameters of the calculated structures, illustrating the role of the entropy factor in the processes under consideration. Δ*H* and Δ*G* of the reaction **1** → **3b** have close values, which indicates an insignificant entropy contribution *T*Δ*S* (−0.4 kcal mol^{-1}). The dissociation of the solvate ligand **3b** → **3a** obviously leads to an

† *Calculation procedure*. Calculations were performed in the Gaussian 16 program[15] within the framework of density functional theory using pure PBEPBE (also known as PBE)[16] and hybrid PBE1PBE (also known as PBE0)[17] functionals. Grimme's dispersion with Becke–Johnson damping (GD3BJ)[18] was added for a more accurate calculation of the dispersion interaction. Def2SVP and Def2TZVP basis sets (including effective core potential, representing 28 core electrons of Pd atom) were used for all atoms.[19] The calculations were carried out in the gas phase and in the presence of a solvent by placing the solute in a cavity within the solvent reaction field (both PCM and SMD formalisms were employed). DMF was taken as a solvent. Hessian calculations were performed for all compounds to ensure that the structures corresponded to the correct point on the potential energy surface, *i.e*. the minimum for the ground states and the saddle point for the transition states. All QTAIM calculations were performed using AIMAll software.[20]

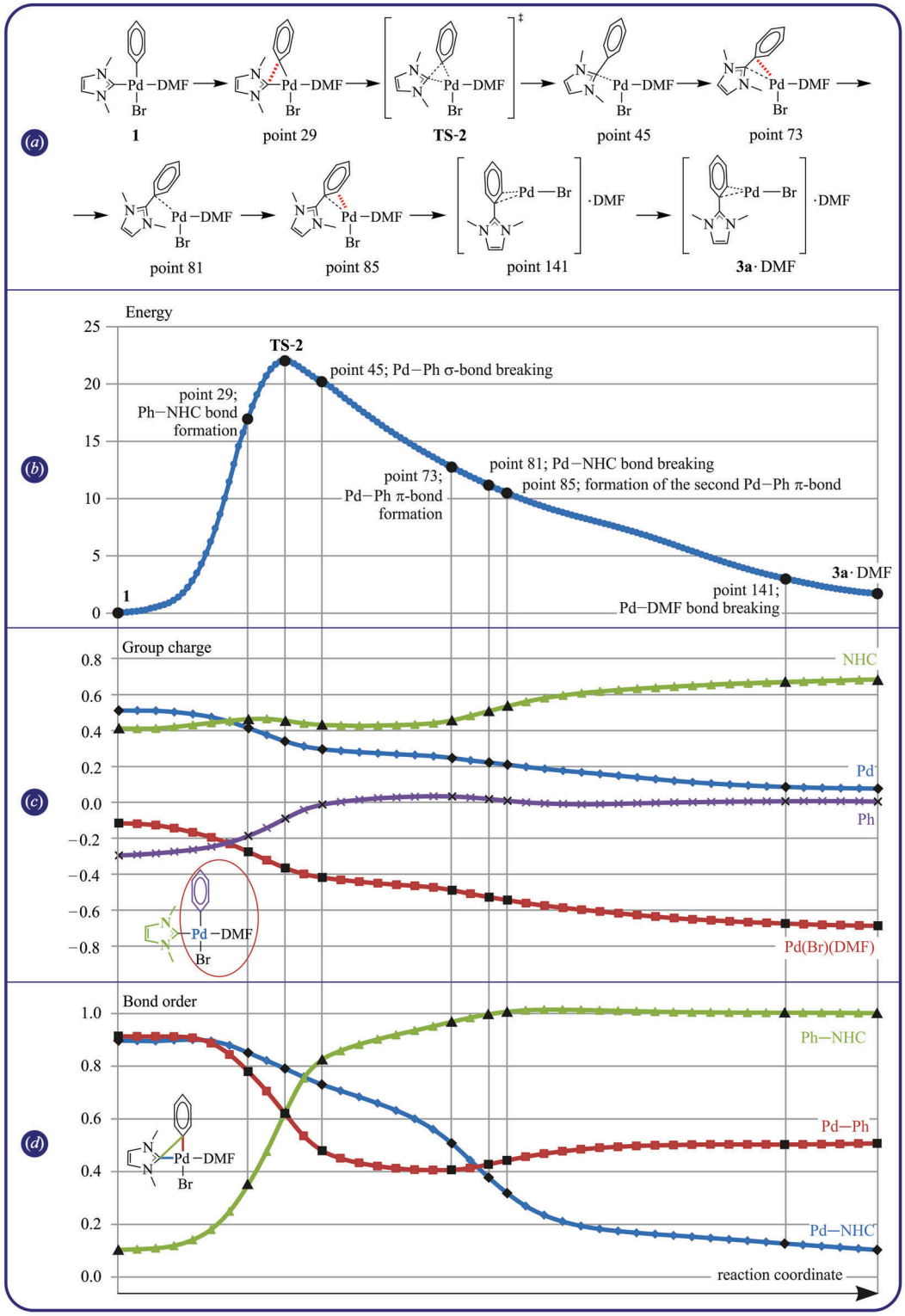

Figure 1 Structural and electronic rearrangements during R–NHC coupling. (*a*) Key points of formation or breakage of bonds; (*b*) energy profile of the reaction (kcal mol^{-1}); (*c*) atomic and group Bader charges (arbitrary units); (*d*) Bader bond orders.

increase in the entropy ($T\Delta S$ = 9.5 kcal mol^{-1}); therefore, the free energy is significantly lower than the enthalpy. Note that in this case, the enthalpy of dissociation is also a negative value (−1.1 kcal mol^{-1}). This clearly indicates that the linear configuration of **3** is preferable to the square planar configuration, even if the entropy component is not taken into account. The contribution of the entropy factor to the ligand exchange reactions is small. The free energy of formation of anionic complex **3a** → **4** is 1.6 kcal mol^{-1} lower than the enthalpy (ΔH = 19.6, ΔG = 18.0 kcal mol^{-1}). In contrast, the entropy factor slightly hinders process **3a** → **5** (ΔH = 33.1, ΔG = 34.5 kcal mol^{-1}). Similarly, the formation of cationic complex **3a** → **6a** proceeds with a decrease in entropy (ΔH = 18.1, ΔG = 20.3 kcal mol^{-1}). Both the enthalpy and the free energy of the reaction indicate that the formation of neutral complex **5** is less favorable than the formation of charged compounds.

An intrinsic reaction coordinate calculation (IRC)[11] was performed for R–NHC coupling along with the Hessian matrix for each trajectory point. Since the SMD model is parametrized for the solvation free energies of a large number of compounds, including ions, and well describes the entropy component of

energy, this method was chosen for the calculations. A total of 165 points were calculated. A topological analysis was carried out for every fourth point within the QTAIM framework.[12] As a result, we have obtained a detailed description of the atomic rearrangements and changes in the electronic structure that take place in the process under consideration [Figure 1(*a*)]. The topologies of the key structures of the IRC path are given in the supporting information (Figure S1). At the beginning of the R–NHC coupling (the first 13 points), small rotations of the phenyl and heterocyclic rings occur in such a way that their further approach proceeds with minimal energy losses. On this segment, the energy of the system grows very slowly [Figure 1(*b*)], while the charge on the Pd atom and the group charges of the NHC, Ph, Pd(Br)(DMF) structural fragments practically do not change [Figure 1(*c*)]. The Pd–Ph, Pd–NHC and Ph–NHC bond orders also change slightly [Figure 1(*d*)]. Then NHC and phenyl ligands begin to approach each other (points 13–29). The energy of the molecule increases rapidly, and a new Ph–NHC bond critical point (BCP) appears in the system (structure 29 on the IRC path). In this segment, the total charge on the Pd(Br)(DMF) fragment begins to decrease, while on the Ph and NHC fragments, it begins to increase. As expected, the Pd–Ph and Pd–NHC bond orders begin to decrease. Note that after the formation of the Ph–NHC bond (after the appearance of the corresponding BCP), a slight charge redistribution between the phenyl group and the carbene ligand occurs. As a result, the charge on the phenyl ring begins to increase more rapidly, while the group charge on the heterocyclic fragment decreases. The energy of the system increases up to the point of the transition state (**TS-2**). In the **TS-2** structure, the Pd–Ph and Ph–NHC bond orders are equal, as evidenced by the intersection of the red and green curves in Figure 1(*d*), while the NHC ligand remains firmly bound to the metal. During Ph–NHC coupling, the Pd–Ph bond order decreases faster than the Pd–NHC bond order. This asynchrony is an additional argument in favor of the mechanism of insertion of the phenyl group in the Pd–NHC bond. After the system reaches the transition state, the energy begins to decrease; the distance between the reacting ligands continues to shorten, and the same tendencies of change in charges and bond orders are retained up to point 45, at which point the Pd–Ph BCP disappears. On the segment of the trajectory between points 45 and 73, the approach of the reacting ligands slows down, and the phenyl fragment is oriented in such a way as to form π-coordination with the metal atom. In this phase of the reaction, the charges change only slightly. The decrease in the Pd–NHC bond order and the increase in the Ph–NHC bond order continue. Point 73 is characterized by the appearance of a new BCP Pd–Ph (between Pd and the carbon atom in the *ipso*-position of the phenyl substituent), which we interpret as the formation of a π-complex. This event is followed by the disappearance of the Pd–NHC BCP (point 81) and the appearance of the second Pd–Ph BCP (point 85). A new bond is formed with the *ortho*-C atom of the phenyl ring. After point 73, the Ph–NHC interatomic distance does not change. The decrease in energy in the segment between points 73 and 85 occurs due to the formation of a more favorable π-coordination of Ph–NHC and the palladium atom. The final stage of the reaction is associated with the previously considered transition of the Pd^0 atom from the square-planar configuration to the linear configuration (**3b** → **3a**). As a result, the solvate ligand is pushed out of the metal coordination sphere (point 85–point 141) to form an associate between complex **3a** and the solvate molecule. The decrease in energy after the disappearance of the Pd–DMF bond (point 141) is associated with a change in the mutual orientation of **3a** and DMF and the formation of a more favorable associate.

In addition to the data presented, we plotted bond energy *versus* reaction coordinates for key chemical bonds using the Espinosa–Lecomte–Molins correlation (Figure S2).[13] The results obtained also indicate that the R–NHC coupling reaction is an insertion of a phenyl group into the Pd–NHC bond, since the Pd–NHC bond energy decreases from 67.6 to 63.1 kcal mol^{-1} upon transition from the reagent to the transition state, while this parameter for the Pd–Ph bond decreases much more strongly (from 54.7 to 42.1 kcal mol^{-1}).

The σ- and π-complexes of the palladium atom with the phenyl ring within the QTAIM framework are easily distinguished by the ellipticity parameter (ε) in the BCPs. Thus, ε of the Pd–Ph bond in σ-complex **1** is only 0.03, while in the π-product **3a**·DMF, the ellipticity of two Pd–Ph bonds with *ipso* and *ortho* carbon atoms is 1.94 and 0.66, respectively. The bond between Pd and *ortho*-C atoms is stronger, as evidenced by the values of the electron density in the BCPs: 0.092 a.u. (*ipso*-C–Pd) and 0.099 a.u. (*ortho*-C–Pd).

Modelling of the off-cycle process of R–NHC coupling, which occurs in the intermediates of the Mizoroki–Heck and cross-coupling reactions, was carried out. This process is exergonic, and its potential barrier is low for the conditions of the vast majority of catalytic reactions. During R–NHC coupling, the most weakly bound solvate ligand is displaced from the palladium coordination sphere. The R–NHC coupling mechanism is the insertion of an organic ligand in the Pd–NHC bond. A detailed analysis of the reaction coordinate and calculations of intermediate structures by the QTAIM made it possible to determine the key points of the reaction path: Ph–NHC bond formation, transition state, Pd–Ph bond breaking, Pd–Ph bond formation, Pd–NHC bond breaking, formation of the second Pd–Ph bond, and Pd–DMF bond breaking. It has been shown that charge redistribution occurs during the reaction. The group charge of the structural fragment [Ph–NHC] increases by approximately 0.6 a.u., and the charge of the fragment [(DMF)Pd(Br)], respectively, decreases by the same amount.

To summarize, we can compare the classical C–C coupling process on the example of two Ar groups (the process extensively studied in the literature for Pd complexes, see, for example ref. 14) and Ar–NHC coupling studied in detail here (Scheme 3). These reactions, similar at first glance, differ in a number of ways. The most obvious feature is the difference in coupling ligands. In the case of Ar–Ar coupling both reactive ligands are anionic, *i.e.* oxidizing the metal center. In the Pd–NHC complex, one anionic (Ar) and one neutral (NHC) ligand are coupled. However, the latter process also results in the formation of the

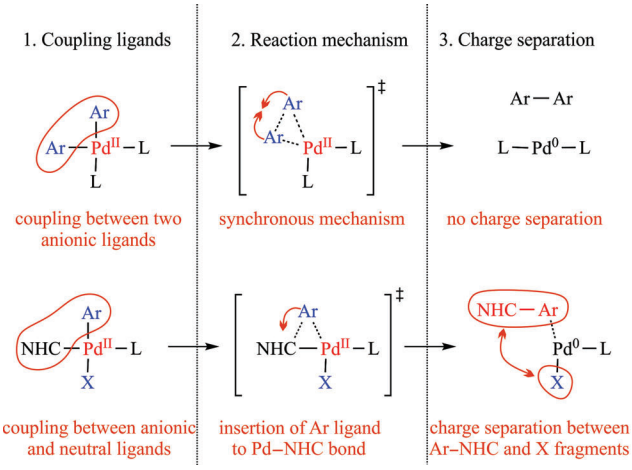

Scheme 3 Comparison of Ar–Ar and Ar–NHC coupling reactions. Atoms or ligands with a negative oxidation state are indicated in blue; red indicates a positive oxidation state.

Pd^0 complex (rather than the Pd^I complex) due to the transfer of an electron from the neutral ligand to the palladium atom. The next important difference between the two processes under consideration is the reaction mechanism. According to the literature data, the coupling reaction of two Ar ligands proceeds synchronously. Both Pd–Ar bonds in the transition state are elongated by the same value. The Ar–NHC coupling, as defined in the present study, is an insertion of the Ar ligand into the Pd–NHC bond. The Pd–NHC bond lengths in the transition state and in the reagent have almost the same values. The last distinguishing sign is a consequence of the electron transfer from the NHC to the metal atom. As a result, charge separation occurs in the coupling product: the Ar–NHC fragment is formally positively charged, while the anionic ligand X bound to palladium is negatively charged. The charge separation in the complex opens the way for further dissociation with the possibility of the formation of cationic, anionic, and neutral Pd^0 compounds.

This work was supported by the Russian Science Foundation (grant no. 20-73-00210).

Online Supplementary Materials

Supplementary data associated with this article can be found in the online version at doi: 10.1016/j.mencom.2022.09.001.

References

1 A. J. Arduengo, III, R. L. Harlow and M. Kline, *J. Am. Chem. Soc.*, 1991, **113**, 361.

2 W. A. Herrmann, M. Elison, J. Fischer, C. Köcher and G. R. J. Artus, *Angew. Chem., Int. Ed.*, 1995, **34**, 2371.

3 (*a*) Z. Wang, N. V. Tzouras, S. P. Nolan and X. Bi, *Trends Chem*., 2021, **3**, 674; (*b*) A. Collado, D. J. Nelson and S. P. Nolan, *Chem. Rev.*, 2021, **121**, 8559; (*c*) A. H. Hoveyda, Y. Zhou, Y. Shi, M. K. Brown, H. Wu and S. Torker, *Angew. Chem., Int. Ed.*, 2020, **59**, 21304; (*d*) D. Balcells and A. Nova, *ACS Catal.*, 2018, **8**, 3499; (*e*) Q. Zhao, G. Meng, S. P. Nolan and M. Szostak, *Chem. Rev.*, 2020, **120**, 1981; (*f*) K. Riener, S. Haslinger, A. Raba, M. P. Högerl, M. Cokoja, W. A. Herrmann and F. E. Kühn, *Chem. Rev.*, 2014, **114**, 5215.

4 (*a*) C. Valente, S. Calimsiz, K. H. Hoi, D. Mallik, M. Sayah and M. G. Organ, *Angew. Chem., Int. Ed.*, 2012, **51**, 3314; (*b*) S. Shi, S. P. Nolan and M. Szostak, *Acc. Chem. Res.*, 2018, **51**, 2589; (*c*) R. D. Froese, C. Lombardi, M. Pompeo, R. P. Rucker and M. G. Organ, *Acc. Chem. Res.*, 2017, **50**, 2244; (*d*) G. C. Fortman and S. P. Nolan, *Chem. Soc. Rev.*, 2011, **40**, 5151.

5 (*a*) H. Jacobsen, A. Correa, A. Poater, C. Costabile and L. Cavallo, *Coord. Chem. Rev.*, 2009, **253**, 687; (*b*) S. Díez-González and S. P. Nolan, *Coord. Chem. Rev.*, 2007, **251**, 874.

6 (*a*) K. J. Cavell and D. S. McGuinness, *Coord. Chem. Rev*., 2004, **248**, 671; (*b*) D. J. Nelson, J. M. Praetorius and C. M. Crudden, in *N-Heterocyclic Carbenes: From Laboratory Curiosities to Efficient Synthetic Tools*, 2nd edn., ed. S. Diez-Gonzalez, Royal Society of Chemistry, London, 2017, pp. 46–98.

7 A. V. Astakhov, O. V. Khazipov, A. Yu. Chernenko, D. V. Pasyukov, A. S. Kashin, E. G. Gordeev, V. N. Khrustalev, V. M. Chernyshev and V. P. Ananikov, *Organometallics*, 2017, **36**, 1981.

8 V. M. Chernyshev, E. A. Denisova, D. B. Eremin and V. P. Ananikov, *Chem. Sci.*, 2020, **11**, 6957.

9 G. Scalmani and M. J. Frisch, *J. Chem. Phys.*, 2010, **132**, 114110.

10 A. V. Marenich, C. J. Cramer and D. G. Truhlar, *J. Phys. Chem. B*, 2009, **113**, 6378.

11 (*a*) K. Fukui, *Acc. Chem. Res.*, 1981, **14**, 363; (*b*) H. P. Hratchian and H. B. Schlegel, in *Theory and Applications of Computational Chemistry: The First 40 Years*, eds. C. E. Dykstra, G. Frenking, K. S. Kim and G. Scuseria, Elsevier, Amsterdam, 2005, ch. 10, pp. 195–249.

12 R. W. F. Bader, *Atoms in Molecules: A Quantum Theory*, Clarendon Press, Oxford, 1994.

13 E. Espinosa, E. Molins and C. Lecomte, *Chem. Phys. Lett*., 1998, **285**, 170.

14 (*a*) M. Pérez-Rodríguez, A. A. Braga, M. Garcia-Melchor, M. H. Pérez-Temprano, J. A. Casares, G. Ujaque, A. R. de Lera, R. Álvarez, F. Maseras and P. Espinet, *J. Am. Chem. Soc.*, 2009, **131**, 3650; (*b*) V. P. Ananikov, D. G. Musaev and K. Morokuma, *Eur. J. Inorg. Chem*., 2007, 5390; (*c*) J. F. Hartwig, *Inorg. Chem.*, 2007, **46**, 1936; (*d*) K. Osakada, H. Onodera and Y. Nishihara, *Organometallics*, 2005, **24**, 190; (*e*) V. P. Ananikov, D. G. Musaev and K. Morokuma, *Organometallics*, 2005, **24**, 715.

15 M. J. Frisch, G. W. Trucks, H. B. Schlegel, G. E. Scuseria, M. A. Robb, J. R. Cheeseman, G. Scalmani, V. Barone, G. A. Petersson, H. Nakatsuji, X. Li, M. Caricato, A. V. Marenich, J. Bloino, B. G. Janesko, R. Gomperts, B. Mennucci, H. P. Hratchian, J. V. Ortiz, A. F. Izmaylov, J. L. Sonnenberg, D. Williams-Young, F. Ding, F. Lipparini, F. Egidi, J. Goings, B. Peng, A. Petrone, T. Henderson, D. Ranasinghe, V. G. Zakrzewski, J. Gao, N. Rega, G. Zheng, W. Liang, M. Hada, M. Ehara, K. Toyota, R. Fukuda, J. Hasegawa, M. Ishida, T. Nakajima, Y. Honda, O. Kitao, H. Nakai, T. Vreven, K. Throssell, J. A. Montgomery, Jr., J. E. Peralta, F. Ogliaro, M. J. Bearpark, J. J. Heyd, E. N. Brothers, K. N. Kudin, V. N. Staroverov, T. A. Keith, R. Kobayashi, J. Normand, K. Raghavachari, A. P. Rendell, J. C. Burant, S. S. Iyengar, J. Tomasi, M. Cossi, J. M. Millam, M. Klene, C. Adamo, R. Cammi, J. W. Ochterski, R. L. Martin, K. Morokuma, O. Farkas, J. B. Foresman and D. J. Fox, *Gaussian 16, Revision C.01*, Gaussian, Wallingford, CT, 2016.

16 J. P. Perdew, K. Burke and M. Ernzerhof, *Phys. Rev. Lett*., 1996, **77**, 3865.

17 C. Adamo and V. Barone, *J. Chem. Phys*., 1999, **110**, 6158.

18 S. Grimme, S. Ehrlich and L. Goerigk, *J. Comput. Chem.*, 2011, **32**, 1456.

19 F. Weigend and R. Ahlrichs, *Phys. Chem. Chem. Phys*., 2005, **7**, 3297.

20 T. A. Keith, *AIMAll, Version 19.10.12*, T. K. Gristmill Software, Overland Park, KS, USA, 2019 (aim.tkgristmill.com).

Received: 29th April 2022; Com. 22/6887